

Chapter 1

Plasmon Interactions in Tip Dimers

The final set of experiments discussed in this thesis are the product of each of the developments from previous chapters, utilising pairs of tips in the microscope platform to investigate the limits of plasmon coupling. Coupling between different tip morphologies is dynamically investigated to both confirm plasmonic behaviour in tips and increase understanding of the characteristic regimes of plasmon coupling, including the recently uncovered quantum regime. Through this work an improved interpretation of future results in sub-nm plasmonic gaps can be attained.

1.1 Experimental Measurements of Dynamic Tip Dimers

Dynamic interactions and separation-dependent phenomena between two tips are spectroscopically studied using an axial scanning approach. Tips are coupled with another tip in order to maximise optical accessibility to the gap. Although not representing the typical geometry used in TENOM this presents a more optimal geometry to explore plasmonic coupling on a more fundamental level. Tips are first aligned into the dimer configuration under the supercontinuum laser beam using the capacitive technique described in chapter ???. Alignment takes place with the laser illumination on to prevent spatial changes to the tip apices, caused by thermal expansion, from occurring post-alignment when spectroscopy is performed.¹ The tip of the harder cantilever of the pair is partially positioned in the laser spot and the tip of the softer cantilever is resonantly driven and used as the alignment probe, beginning at distances outside of the laser focus. Sufficient space is left after placement of the stationary tip to accommodate both tip apices equally under the laser spot once brought together. This level of positioning is subjective, with scattering intensity used to estimate an acceptable position for the stationary tip within the collection spot. Once alignment is complete the separation between tips is reduced from around ~ 300 nm to geometrical contact whilst undergoing measurement.

The tips used in experiments, whether commercial or fabricated in-house, are required to

¹This behaviour was briefly looked at, with laser-induced cantilever deflection being measured in tips. This suggested that the heat of the focus was causing mechanical deforming or bending of the AFM probe, moving the lateral position of the tip apex and misaligning the tip dimer prior to gap coupling experiments.

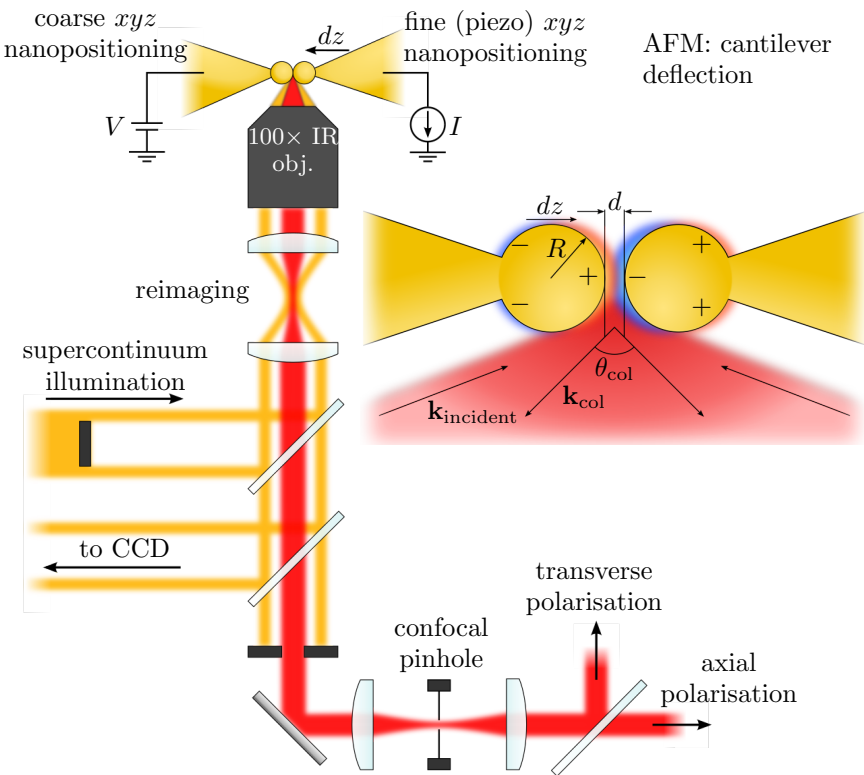


Figure 1.1: Experiment configuration for axial tip scanning. The laser is centred on the aligned tip dimer for gap spectroscopy. The soft cantilever approaches the stationary, stiff cantilever at a rate $dz \text{ nm s}^{-1}$. A bias is applied across the tip junction and the current through the gap is measured. The soft cantilever faces the AFM module for force measurement via cantilever deflection. A diagram of tip dimer characteristics is shown as an inset. The diagram specifically shows the case for a spherical Au tip dimer, showing the antenna plasmon modes which couple together. Plasmonic coupling depends on both the gap size, d , and the particle radius, R , where the mobile tip particle approaches a stationary spherical tip at a rate dz . The illumination and collection angles, defining $\mathbf{k}_{\text{incident}}$ and \mathbf{k}_{col} , are $\theta_{\text{incident}} = \sin^{-1}(0.6 - 0.8NA)$ and $\theta_{\text{col}} < \sin^{-1}(0.6NA)$.

have clean metallic surfaces when studying gap plasmon interactions. Layers of insulating surface molecules only prevent the gap from narrowing sufficiently to enter the quantum regime. Any layers deposited as either a byproduct of a chemical reaction or carbon deposition in SEM need to be removed. This is done through either plasma cleaning or piranha treatment. To maintain cleanliness some experiments are performed in a nitrogen flow environment.

During scanning measurements on tip dimers, the stationary tip acts as the optical probe, staying fixed in the collection spot throughout the scan, whilst the other tip approaches at a rate of $0.1\text{--}1 \text{ nm s}^{-1}$. Approach speeds are continually adjusted and optimised during scanning to reduce the time interval between completion of alignment and achieving geometrical contact and minimise any potential lateral drift. Use of a stiffer cantilever ensures that the AFM tip remains fixed in its current position under the laser spot, even once under pressure from the opposite tip. Measurements of the optical scattering, electronic conductance and applied force are taken at each point in the scan. The geometry of this experiment is shown in Figure 1.1.

The approaching tip perturbs the near-field and interacts with the probe tip. Separation-dependent optical scattering is then collected through the objective collection aperture. Strong scattering of the intense supercontinuum source means 10–20 ms integration times are sufficient for a high quality signal to noise, therefore spectra acquisition does not affect the scan speed. Only light polarised along the tip dimer axis is reported in the context of this work in order to focus on the influence of charge transfer on bonding hybridised plasmons.

Simultaneous measurement of gap conductance and applied force supplement optical scattering measurements, enabling correlations to be made between characteristic gap properties to better interpret the relationship between charge transfer and plasmonic coupling.² Electronic properties are probed by driving with a d.c. voltage and measuring the current through the tip junction to determine its conductance. A bias of 50 mV is almost always used to achieve good signal quality in both low-bandwidth and high-bandwidth conductance measurements and to prevent spikes in the noise from setting off the high-bandwidth trigger. Larger voltages increase the electrostatic pull between tips, visible in force measurements, and the resulting high current upon contact would damage tips if not for the current limiting resistor. The smallest current range is fixed at 10 nA, with a sensitivity of 10 fA, since lesser ranges require longer settling times, slowing the scan rate. At 50 mV the smallest measurable conductance is around $10^{-7}G_0$.

The applied force is measured using optical detection of cantilever deflection by the AFM module. At each step in the scan the position of the returning laser beam is averaged for 100 ms to determine the mean cantilever deflection, and therefore the mean applied force, over the duration of electronics and optics measurements. Using this combination of measurements allows for a more informed interpretation of nanoscale gap behaviour than by measuring only the optical scattering, as was done originally [1].

1.1.1 Non-Optical Properties of a Nano-Tip Dimer Gap

Before studying the optical properties of nano-gaps it is beneficial to understand the range of physical phenomena that exist on each characteristic length scale present during scans that traverse from ~ 100 nm to 0.1 nm. With tips well separated, only the separation and optical scattering are meaningful physical quantities. The optical scattering, if plasmonic in origin, is subject to a separation-dependent capacitive interaction. There is no current and no applied force until the separation reduces to below $\mathcal{O}(10)$ nm. Below this point both the current and the force become instrumental in understanding the optical response. Due to the maturity of AFM, STM and molecular electronics there is already a wealth of information explaining both

²Each measurement is ran in parallel using multiprocessing in the experiment control method, with each taking a fixed amount of acquisition time. Multiprocessing not only allows data to be acquired around the same time but also decreases the overall measurement time.

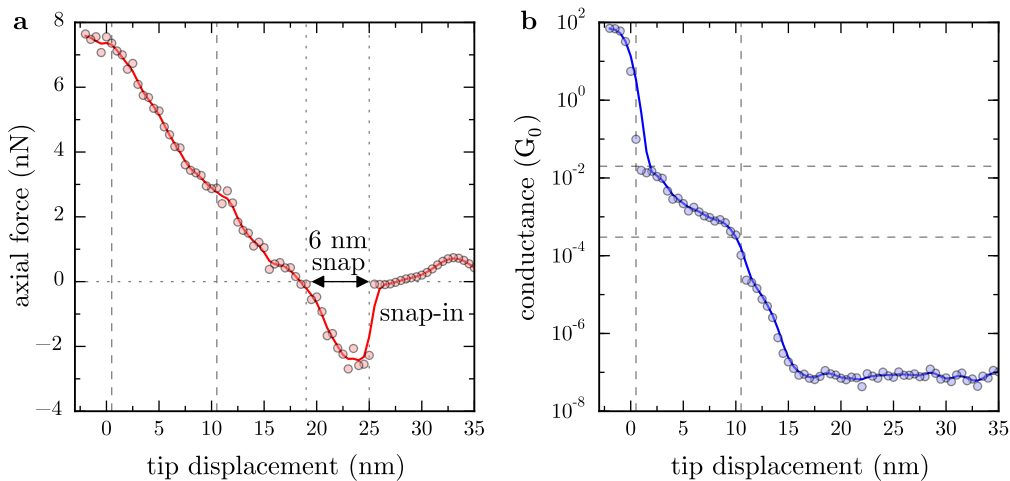


Figure 1.2: Axial force and conductance measurements of a sharp Au tip dimer approaching into contact. The characteristic AFM snap-in effect is seen in the axial force (a) as a discontinuous jump before the linear application of force in a soft contact regime. The tip apices snap together, reducing the separation to on the order of 1 nm, leading to the onset of quantum tunnelling, and finally conductive contact, upon further decreasing the gap separation (b). Dashed and dotted lines are added as guides to the eye showing different features in the scan, such as snap-in and conductance behaviour.

electronic effects and the forces expected on these length scales.

Figure 1.2 shows the conductance and axial force measurements from a typical scan once separation has passed below 10 nm. The force shows no features until there is a fast negative (attractive) jump in the applied force, showing that the tip has been pulled towards the opposing tip (Figure 1.2a). This is the signature of water in gap. The lack of a tunnelling current at this point shows that tips must still be separated by more than 1 nm. The actual extent of these snaps varies between scans depending on a number of factors, including the humidity, with some scans snapping in closer than 1 nm.

Since experiments are carried out in ambient conditions the surfaces of tips will always be coated in a thin film of water or nanobubbles. Even in a nitrogen environment, its presence is only reduced and not completely removed. When two surfaces come into close proximity a water meniscus forms between them, leading to strong capillary forces [2]. Hence, when the separation between the two tips reduces past the point of meniscus formation they are quickly pulled together [3]. This is known in AFM as the “snap-in” or “snap-into-contact” and occurs on separations \sim 5–30 nm [3, 4]. In the above scan the snap distance can be inferred from the displacement required to remove the applied force as 6 nm.

To prevent snap-in either a stiffer cantilever must be used (normally in tapping mode) [5] or the water meniscus has to be removed, which is usually achieved through liquid immersion AFM [4, 6, 7] or by using plasma treatment to remove hydrophobic contamination [4]. In this instance, however, the water layer is advantageous. The presence of the meniscus prevents immediate electrical and geometrical contact and holds tips around 1 nm apart until further

force is applied. Approach of the tips then occurs in much finer increments due to mechanical resistance from the water. This effectively splits a scan into three regimes - one in which the decreasing intertip separation is directly controlled, one after snap-in where cantilever displacement gradually pushes the tip through the water meniscus (soft interaction), and finally one in which force is applied directly to the opposite tip in geometrical contact (hard-wall contact).

The existence of the soft interaction regime enables sub-nm gaps to be studied with some degree of control since only a fraction of the applied cantilever displacement corresponds to a displacement at the apex. Instead, the meniscus is loaded with an applied force, leading to the linear reverse deflection observed in AFM force measurements. This can be seen in Figure 1.2 where 15 nm of cantilever displacement moves the apex \sim 0.8–0.9 nm (deduced from electron tunnelling measurements). The remaining 14.2 nm loads the gap with 8 nN of force, proportional to the cantilever's spring constant.

Use of soft AFM probes (contact mode cantilevers) means a greater spatial resolution in the sub-nm regime since force is applied more gently with cantilever displacement.³ Softer cantilevers are also advantageous during tip alignment as they have larger oscillation amplitudes, and therefore lower voltages are needed to reach acceptable signal quality, and also lower bandwidth requirements (13 kHz as opposed to 190–300 kHz). For these reasons, along with those directly related to tip alignment capabilities (outlined in chapter ??), one tip in the dimer is usually a contact mode probe while the other tip, which must remain stationary under an applied force, is a stiffer tapping mode probe. Early experiments exclusively used contact mode cantilevers until determining that spectral changes could not be guaranteed to originate from the gap under the application of a large force.

Despite their usefulness in showing the relative motion of the tip, force measurements are somewhat limited in their information on the absolute separation. An estimate of the absolute separation is made possible by studying charge transfer in the gap. Electron tunnelling is the dominant charge transfer mechanism, occurring prior to conductive contact with the current due to tunnelling follows an approximately exponential decay with increasing separation. The conductance in STM is often stated to drop by approximately a factor 10 for every 1 Å away from conductive (approximately geometrical) contact. This relation permits deduction of the gap separation to a certain degree using the order of magnitude of the gap conductance.

Upon reducing the gap to below 1 nm electron tunnelling becomes detectable. Though the absolute value of the conductance for a given separation depends on the gap morphology the relative exponential conductance drop from geometrical contact still approximately holds for $d > 2 \text{ \AA}$ [8]. This makes electron tunnelling a useful method for estimating the gap size to within \sim 0.1 nm. Once the separation is greater than 1 nm the conductance drops to

³Smaller k means larger x required for $F = kx$ to meet the same target value.

below around $10^{-9}G_0$ and the corresponding current becomes difficult to measure without significantly raising the d.c. bias. For example, use of a 50 mV bias means a current on the order of 1 fA, which remains below the currently achievable noise level.

Figure 1.2b shows a typical conductance trace on approach. Once the separation decreases below 1 nm the conductance steadily increases with force from 10^{-7} to around $10^{-4}G_0$ as the tips transition through the soft interaction regime. At $10^{-4}G_0$, the rate of conductance increase slows, signifying the compacting of the meniscus into a single monolayer of water, which requires a greater force to displace. At $10^{-2}G_0$ the separation is estimated to be similar in size to a single water molecule (2.75 Å), which, when displaced, causes tips to quickly transition into geometrical contact, saturating with a contact conductance around $100G_0$. The displacement of this final gap layer and consequent relief of force on the tip is shown by a decrease in the force gradient during the transition into contact.

Each of the electronic and force measurements described in this section are instrumental in discerning the underlying phenomena occurring in sub-nm gaps. These measurements can then be correlated with optical spectra and used to interpret changes to plasmon coupling, especially changes that depend sensitively on gap morphology or dielectric medium. Using this information, more accurate physical models can be developed to further understand the quantum regime of plasmon coupling than what currently exist.

1.2 Plasmonic Coupling Between Tips

Plasmonic interactions between tips are studied using the dimer approach. Two AFM tips are dynamically brought together to form a single gap structure, mimicking a plasmonic dimer cavity, whilst the optical scattering, conductance and force are simultaneously measured. The resulting experiment geometry is shown as an inset in Figure 1.1. Both sharp and spherical Au tips are studied in a range of dimer permutations, in order to understand how plasmons in each tip couple. This is also compared with results from hyperspectral characterisation, indicating whether plasmons initially exist in such structures.

1.2.1 Sharp Tip Dimer Interactions

The first combination of AFM tips studied is a sharp Au tip interacting with another sharp Au tip. Hyperspectral characterisation indicates that sharp Au tips lack any observable LSPs. Similarly for dimer experiments, no observable coupling is expected, despite the possibility that gap modes may exist. Reducing the separation between two sharp Au tips indeed shows no resonances or coupled modes (Figure 1.3). Scattering increases are seen, however these do not shift with decreased separation or change with conductance. They are instead attributed to

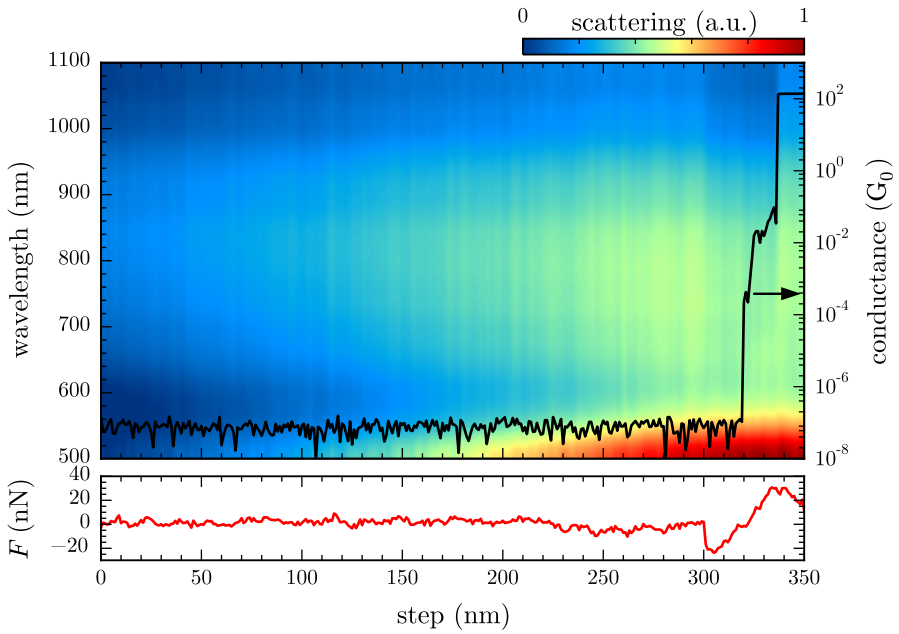


Figure 1.3: Spectra of a sharp Au tip approaching a stationary sharp Au tip. Sharp Au tips are BudgetSensors GB series AFM probes. There are no identifiable plasmon resonances initially in the system and no new modes appear with decreasing gap size. The lack of any shifting suggests that plasmons are not present in the system. The increase in intensity and its spectral shape are an artefact of adding more of the reflective tip facet into the confocal collection aperture.

more of the reflective tip facet entering the confocal collection aperture as the tip is approached to the stationary tip. The superimposed spectral scattering increase also bears resemblance to the spectral density of the illumination, further supporting this claim. Correlations between the scattering intensity and the torsional force also support this explanation.

Tunnelling currents are observed to have no effect on scattering from the gap, despite reports suggesting that tunnelling electrons excite plasmons [9–14]. The reason for this is the small 50 mV bias. The excitation condition $\hbar\omega < eV$ is not satisfied for visible frequencies and hence only low energy SPPs in the IR could be excited.⁴ Using higher voltages around 2 V would give a finite probability that an electron would excite an SPP, with intensity depending on the current through the junction and the collection geometry.⁵ In the current geometry only localised gap modes could be observed since the system lacks a means of measuring SPP leakage radiation. Furthermore, reports detecting radiation from localised gap modes have used sensitive CCDs with long integrations. Hence, within this system when using 10 ms integration times, it is unlikely that tunnelling-induced radiation will be detected.

The conclusions drawn from these experiments agree with those of individual sharp Au tip spectroscopy. Sharp Au tips do not show any evidence of supporting plasmons which readily

⁴For a 50 mV voltage the limiting frequency is 7.6×10^{13} rads, or $\lambda = 24.8 \mu\text{m}$ deep in the IR.

⁵For a 2 V voltage the limiting frequency is 3.0×10^{15} rads, or $\lambda = 630 \text{ nm}$. Hence plasmons can be excited in the red frequencies of the visible spectrum and below.

couple with light and there have been no detected signatures of plasmon coupling between similar tips. However, both the gap geometry and previous spectroscopic (spectroscopy, TERS and electrical excitation) measurements on tips suggest that plasmons and gap modes can exist in such geometries. It can only be stated that, based on the measurements shown here, only radiative antenna-like plasmons can be seen in the far-field and that tips are not capable of supporting these. Further tests outside the scope of the work discussed in this thesis would be required to test for SPP excitation and how these effect the underlying mechanisms of TENOM.

In order to optically probe plasmon coupling in a sub-nm cavity between two tips, a tip geometry is required that strongly interacts with far-field light. Sharp Au tips are clearly inadequate for this purpose. For this reason the spherical tip geometry, with its visible wavelength plasmon resonances, facilitates the dynamic study of plasmonic coupling in nanoscopic gaps.

1.2.2 Spherical Tip Dimer Interactions

By using spherical Au tips the tip-tip system mimics the prototypical spherical AuNP dimer. It is through this arrangement that a controllable plasmonic dimer is recreated. The presence of far-field-coupled, antenna-like plasmons, discussed in chapter ??, enables the detection of gap modes as tips transition from the non-interacting regime at $\sim 300\text{ nm}$ through into the charge transfer regime before entering conductive contact. By utilising such a controllable plasmonic system, plasmon coupling can be better understood on a fundamental level and unravel the remaining questions regarding plasmonics in sub-nm gaps.

Spherical Tip Interactions with a Spherical Tip

The first configuration of spherical tips studied is that of a spherical Au tip approaching another spherical Au tip. In this instance the 600–650 nm LSPs of the individual tips interact and form observable hybridised gap modes. Representative scans of two approaching spherical Au tips are shown in Figure 1.4, in which plasmon resonances are dynamically followed from non-interacting to classically hybridised. It should be noted that in previous microscope designs the short-range tip alignment meant that plasmons were only observed once coupled near 750 nm [1]. Improvements to the range of the tip alignment technique using optical detection have allowed the full range of plasmon coupling to be studied.

Coupling between spherical tips appears very similar to that of a large nanoparticle dimer. Plasmons are initially uncoupled and only the single LSP of the probed tip is observed. Plasmons begin to interact at $d \approx R_{\text{tip}} = 150\text{ nm}$ as is classically expected, where d is estimated based on the point of snap-in. As the gap width decreases the individual plasmon modes hybridise, redshifting monotonically and scattering increasingly. The initial plasmon mode at

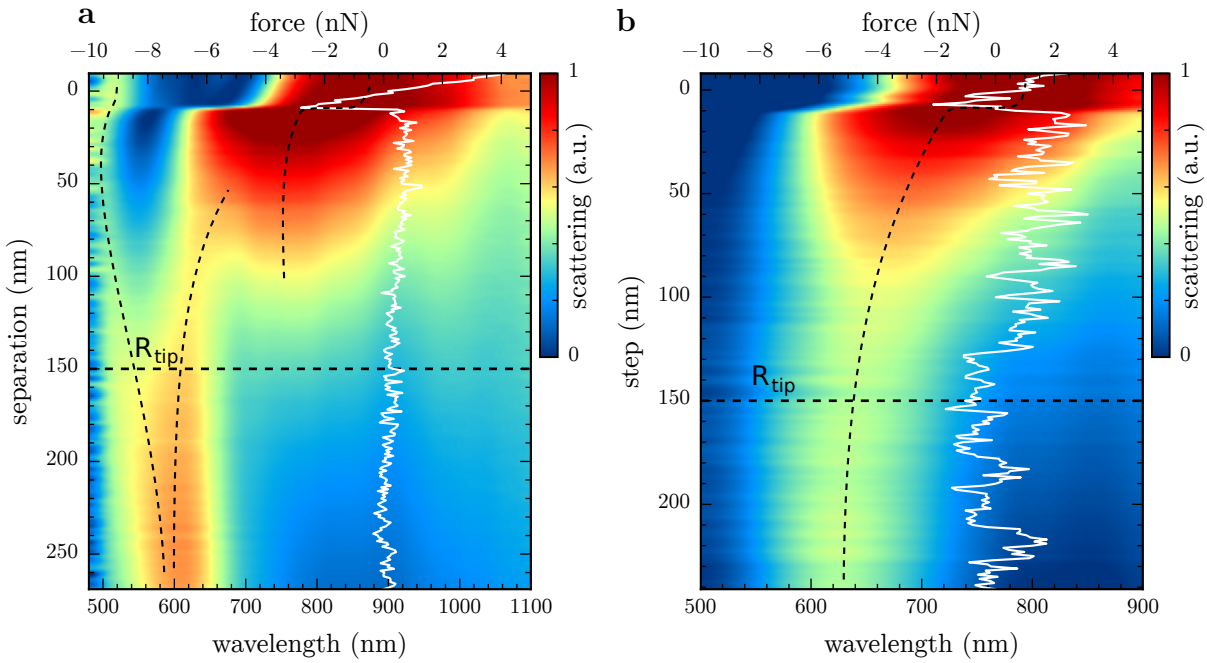


Figure 1.4: Spectra of a spherical Au tip approaching a stationary spherical Au tip. Spherical Au tips are Au-coated NanoTools B150 AFM probes. Two scans are presented in the classical interaction regime, showing similar phenomena. The separation is estimated based on known tip displacements to the point of snap-in. Guides to the eye are added to highlight mode behaviour. Horizontal dashed lines indicate the radius separation, at which point coupling is expected to begin. In both cases, but more clear in (b) with tips having similar initial LSPs, bonding hybridised modes form, which redshift with decreasing intertip separation (increasing coupling). With slightly dissimilar initial LSPs anti-bonding hybridisation can be seen as a blueshifting mode with decreasing intertip separation.

630 nm redshifts to around 800 nm in each scan at the point of snap-in, where the separation is reduced to around 1 nm. Increased scattering is due to both increasing coupling and an increased amount of scattering metal entering the confocal sampling volume of the objective. Once the gap has decreased sufficiently ($d \ll R_{\text{tip}}$) the confocal collection argument is negligible as the sampling volume becomes saturated, hence all further changes are due to plasmon coupling in the gap.

For large distances the rate of redshift is dominated by the increase in capacitive coupling as the separation decreases. In each scan a large abrupt redshift of the coupled mode correlates with snap-in. The large redshift on snap-in is due in part to two effects: the decrease in separation as the tip is pulled in by capillary forces and the increase in refractive index as the gap constitution transitions from air to water (and any material contained in the water meniscus). The intensity of the lowest order mode begins to decrease once the gap width decreases below 1 nm. This effect is attributed to the mode becoming increasingly confined to the point of becoming non-radiative. Similar changes in mode intensity are often seen in classical simulations and occur well before the onset of any significant quantum effects [1, 8].

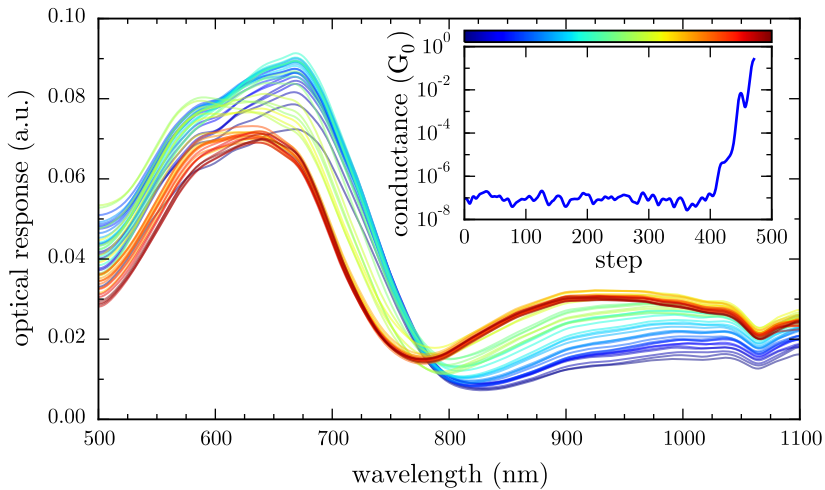


Figure 1.5: Spectra of a spherical Au tip approaching a stationary sharp Au tip. No coupling phenomena are observed due to the mismatch between plasmon modes.

Slightly different classical coupling physics is observed when the dimer symmetry is broken. In some cases where initial tip resonances differ by ~ 50 nm coupling is better described by a heterodimer model rather than a homodimer. Under the asymmetrical condition, anti-bonding modes are no longer dark since dipoles do not exactly cancel. Depending on which particle is probed, either the one supporting the lower or higher energy initial resonance, either a redshifting bonding mode or a blueshifting anti-bonding mode is observed to be the dominant gap resonance (see Figure ?? and [15]). The tip dimer probed in Figure 1.4a clearly exhibits both mode configurations and is a good representation of what is seen across many additional scans.

This effect has been documented previously [15] but never directly observed dynamically. The anti-bonding configuration is typically non-physical in most plasmonic systems since both particles are driven with the same phase of light. However, with larger particles, such as these 150 nm radius spherical Au tips, the phase symmetry is broken allowing anti-bonding hybridised plasmons to be excited. Both the blueshift and the later redshift at small separations are found in spherical tip scans, indicating the interaction and anti-crossing between the lower order anti-bonding mode and the higher order, adjacent bonding mode. The higher order bonding modes responsible for this are then seen after snap-in.

Spherical Tip Interactions with a Sharp Tip

The interaction between the same spherical Au tip and a sharp Au tip is investigated. The results are shown in Figure 1.5. Despite the sharp tip perturbing the field around the spherical tip, acting as the optical antenna, no changes are observed in the spherical tip plasmon, suggesting that there is no interaction between sharp tips and spherical tip plasmons. This is in agreement with predictions that a sharp tip should not deviate the resonance of a planar surface

[16, 17], for which the much larger tip could be considered. The tip acts as a point perturbation not strong enough to significantly modify the more distributed antenna-like response. This observation also supports the measurements shown in chapter ??, where the laser was assumed to stay on resonance with the AuNP tip as it approached the BTh-coated sharp Au tip.

1.3 Quantum Effects in Sub-nm Gaps between Spherical-Tipped AFM Probes

Quantum effects in plasmonic nanogaps become readily observable upon forming a sub-nm gap between spherical tip surfaces. By monitoring the electrical conductivity simultaneously with the optical scattering the effects of quantum charge transfer can be directly inferred under the assumption that the conductance is similar at both d.c. and optical frequencies. Using this approach, the quantum limitations to plasmon coupling are observed in full for the first time. This section discusses the now readily attainable regime of plasmonics in sub-nm gaps. The investigation into the effects of quantum charge transport on plasmon coupling is the culmination of all previous developments to date, yielding some of the most interesting results of this project.

To briefly reiterate theory, according to [18], between separations of ~ 0.3 nm and 1 nm gaps are expected to be in the crossover (tunnelling) regime, a progressive transition into electrical contact where classical theory fails due to the onset of quantum tunnelling. Gaps are characterised by a thin barrier between particles with a growing probability for electrons incident on the barrier to tunnel through it. Non-locality of electrons smears gap surfaces on the quantum level, and long-range interactions round the potential barrier in the gap. Tunnelling-induced charge transfer neutralises charge on the gap surfaces and reduces electromagnetic coupling. This decreases, and eventually halts, the rate of redshift and is otherwise known as the screening effect. Beyond ~ 0.3 nm the increasingly overlapping barrier edges cause the central potential barrier region to drop below the Fermi level, creating a conductive constriction. Ballistic conduction now applies and gaps enter a quantised conductive regime. The increased currents cause hybridised modes to further decouple, blueshifting their resonances as they transform into CTPs.

To date, estimations of a critical separation for the onset of conductive effects vary between 0.2–0.3 nm [1, 8, 18–20] (and in some predictions even larger separations [21]) depending on the specific dimer geometry and materials. However, this is by no means a fundamental quantity and therefore not the most appropriate standard by which to compare experiments. For example, a plasmonic nanogap fixed by a molecular spacer layer can exhibit conductive regime characteristics at much larger gap widths [22, 23]. The critical separation is simply the point at

which rate of charge transfer overpowers capacitive interaction. A set of critical conductances should therefore exist for entry into each respective regime of quantum interaction, irrespective of gap size, that more fundamentally describe the effects of (quantum) charge transport on plasmon coupling.

As theory has previously suggested, critical conductances at optical frequencies are a more appropriate way of describing the regimes of charge transfer behaviour [24, 25]. Experimentally this proves incredibly difficult. In a sense, plasmonics is the only way of measuring an optical conductance. Electronic equipment cannot respond fast enough to measure currents at optical frequencies. One reason as to why charge transfer effects should be understood is therefore to enable the application of plasmonics as a method of measuring conductance at frequencies where standard electronic technologies fail. At this time however, the d.c. current through the gap is measured as an approximation to the true electronic behaviour at optical frequencies and functions as a comparison with the effects seen optically. Using this, the current set of experiments explore the concept of critical conductances as the definitive way of interpreting charge transfer in plasmonic systems.

1.3.1 Observations of Quantum Charge Transport in Plasmonic Cavities

Figure 1.6 shows a selection of spherical Au tip dimer measurements showing both optical and electronic behaviour once in the sub-nm regime. Simultaneous quantum transport and SDF scattering measurements are presented as a function of the applied force compressing the gap. Each set of measurements exhibits the characteristic quantum regime transition between hybridised gap plasmons and charge transfer plasmons. However, comparison between sub-nm gaps formed in different tip dimers proves more difficult as the positions and shifts of plasmon resonances can behave very differently, regardless of any similar agreement between scans in previous coupling regimes. These differences are thought to originate from surface roughness or even smaller differences in nanoscale surface morphology that effect the way optics and electronics couple [18, 21].⁶

Figures 1.6a and 1.6b bear the closest resemblance to recent theory, showing both screening and CTP formation through the quantum regime (the original QCM spectra of sub-nm gaps between spherical Au tips from [1] is replotted in Figure 1.6d with the DFT-calculated conductance density overlaid). Experimental plasmon modes appear at similar wavelengths to QCM predictions. Screening is indicated by a reduction in the rate of redshift and a decrease in scattering intensity. A blueshifting transition between coupled plasmons and emerging CTPs signifies the rise of stronger interparticle currents. The unseen fundamental CTP is expected to exist in the IR, outside the measurable spectral range of the current microscope, though the

⁶Changes in CTP position and intensity are said to originate from the touching profile of the dimer, indicating that the surface roughness may play a role with such large dimer surfaces [18, 21].

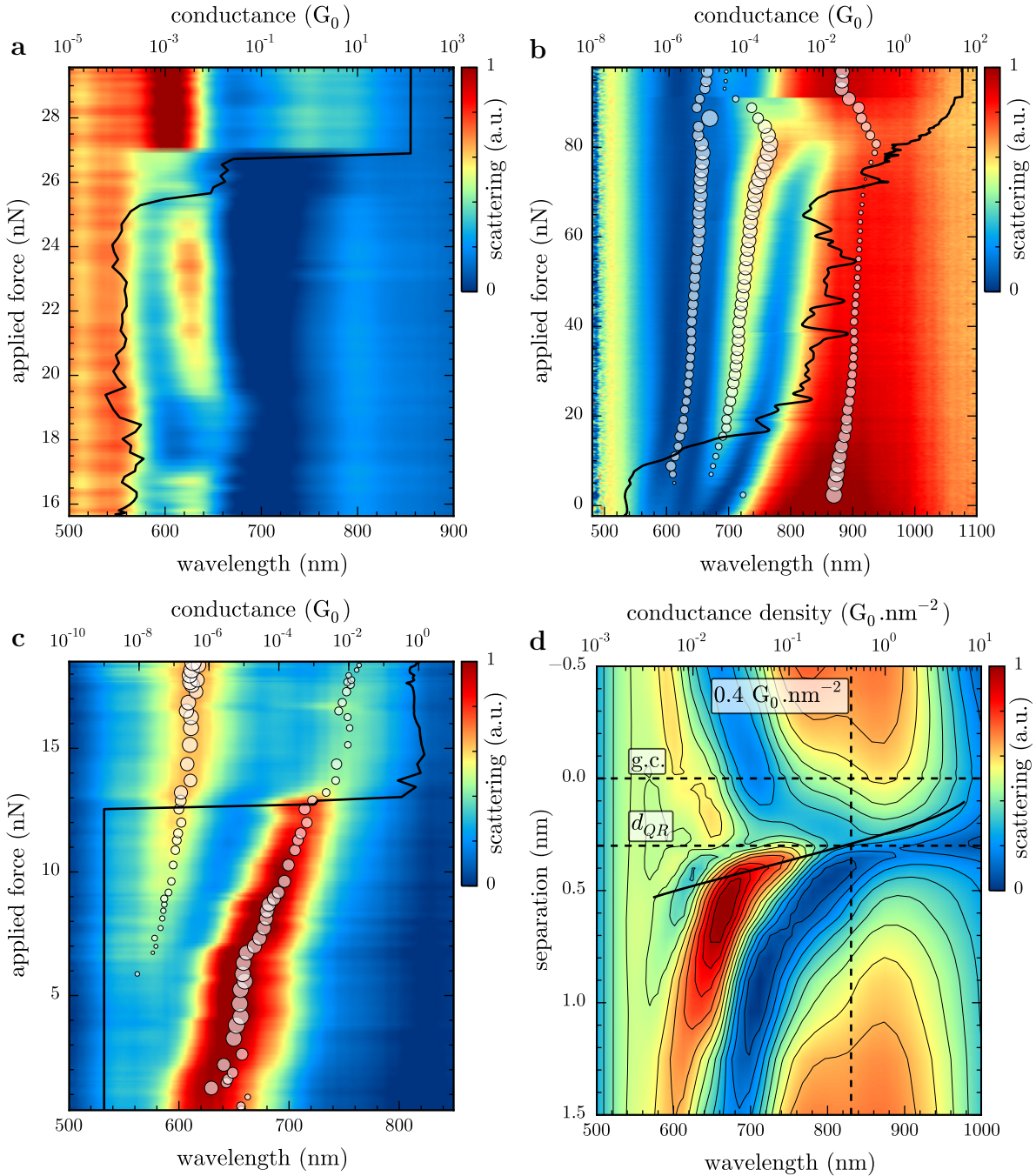


Figure 1.6: Scans of multiple spherical tip dimers passing through the quantum regime and pushing towards geometrical contact. Scans (a–c) show the supercontinuum dark-field scattering spectra as a function of the applied force on the gap with the simultaneously measured conductance superimposed over the axis. The circles highlight the position of the peak. The size of the circle indicates the amplitude of the mode in the fitted model. Scans (a) and (b) use Au-coated NanoTools B150 spherical AFM probes to form a dimer while scan (c) uses electrochemically-fabricated AuNP-on-Pt AFM tips. Calculated QCM spectra of a spherical tip dimer as a function of separation, replotted from [1], is shown in (d). Simulated spectra show that both bonding modes disappear prior to geometrical contact (g.c.) at $d_{QR} = 0.3 \text{ nm}$ and are shortly followed by the rise of CTP modes. This occurs since quantum electronic transport transfers enough charge within half an optical cycle to screen hybridised plasmons and eventually excite a CTP. Based on DFT calculations the CTP is excited when the conductance density is $0.4 G_0 \cdot \text{nm}^{-2}$. These effects are seen in experimental scans once the conductance surpasses $2G_0$.

tip's neck joint may short this mode and prevent its existence. The behaviour of hybridised modes and higher order CTPs is thus used to interpret gap behaviour.

In both experiments, the redshift of each hybridised mode becomes stunted with the onset of tunnelling, revealing that the conductance has risen sufficiently to begin screening gap coupling. The point of blueshift is less clear in Figure 1.6a due to the fast transition into geometrical contact. This jump is experienced in almost all scans and is attributed to a combination of the electrostatic pull between tips and a sudden decrease in mechanical resistance once the water molecules in the gap are displaced. The approach shown in Figure 1.6b is much more carefully controlled going into geometrical contact and provides a much clearer insight into the origins of the blueshift. The scan is likely the single most informative scan, containing many measurements in both the tunnelling and conductive regimes, including clear observation of discretely quantised conductance channels. It is at the transition between tunnelling and ballistic conduction, at around $2G_0$, that the blueshift of plasmon resonances begins to occur and tips enter the quantum conductive regime. This is in good agreement with the principles underpinning recent theoretical models [1, 18].

A better view of this transition is shown in Figure 1.7a with a linear conductance scale in order to closer inspect charge transfer behaviour. The turning point in the redshift of both hybridised plasmons visually appears to occur at $2G_0$. Fitting spectra and extracting the behaviour of each individual mode provides a more quantitative analysis. The results of the fit are superimposed onto spectra in Figure 1.7a with fit parameters shown separately in Figure 1.7b. Mode positions approximately follow an exponential model as expected. At $2 \times 10^{-3}G_0$ the plasmon redshifts, along with their amplitudes and widths, deviate from this model and becomes less pronounced. Prior to this point the amplitude of the lower order mode is decreasing, likely due to increasing charge localisation. Upon passing through this first critical conductance at $2 \times 10^{-3}G_0$ the amplitude is further screened and decreases faster. The higher order mode continues to gain intensity at this point, potentially from redistributed charge of the lowest order mode. Similar behaviour is found in the mode widths. This is the tunnelling regime of plasmonics.

The second critical conductance occurs as $2G_0$ just after transitioning from tunnelling into a quantum conductive regime, i.e. once the Fermi level is above the gap barrier. Upon surpassing $2G_0$ the resonance position of both gap plasmons begins to strongly blueshift into CTPs as current passes through the junction, quickly returning to their initial resonance position prior to entering the tunnelling regime. During this transition the intensity and width of the lowest energy plasmon begins to increase, while the higher order plasmon attenuates into only a weak, blueshifted resonance. This CTP becomes fully developed during the final pull into geometrical contact.

Despite integer quantised conductance being observed in the early conductive regime, there

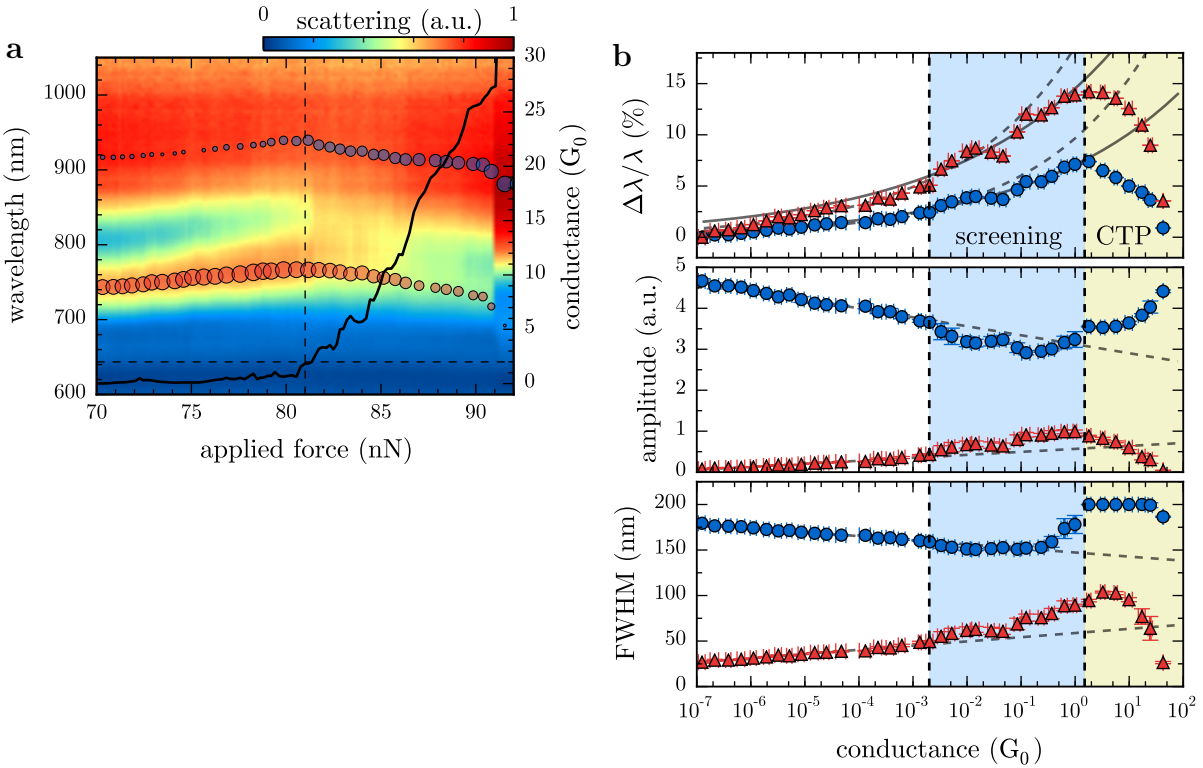


Figure 1.7: Detailed analysis of a spherical Au tip dimer scan in the quantum charge transfer regime. The scan shown in Figure 1.6b is replotted in (a) with a linear conductance scale to show quantised conductance stepping and its relationship with scattering spectra. Dashed lines indicate the point of blueshift at $G = 2G_0$. Peak positions in the fitted model are denoted by circles superimposed onto spectra with their size corresponding to the peak amplitude. The relative shift of each mode from fitted parameters, along with a normalised amplitude and FWHM, are plotted in (b). Vertical dashed lines highlight the transitions into the tunnelling (crossover) regime at $2 \times 10^{-3}G_0$ and the conductive regime at $1.5G_0$. Exponential curves are fitted to the wavelength shift for $G < 10^{-3}G_0$ (dashed) and $G > 2 \times 10^{-3}G_0$ (solid) to highlight the reduction in redshift caused by passing through the screening (tunnelling) threshold. Similar lines are plotted to show changes in the amplitude and width upon passing through $2 \times 10^{-3}G_0$.

is no obvious step-wise shifting of plasmon resonances. It would be intuitive to expect quantised current changes to discretise incremental blueshifts, however this appears not to be the case with the blueshift appearing smooth throughout. More experimental and theoretical data would be needed to properly understand this phenomenon.

Both sets of measurements at the focus of this discussion are not without their issues, however, when compared with both theory and previous experimental results. Figure 1.6a shows variations in both the position and intensity of the 600 nm mode, which are attributed to changes in the torsional force on the gap, corresponding to a rotational motion of the tip. The mode also does not appear to shift as much as expected. The intensities of the final two modes when in contact are also reversed compared with QCM predictions. Figure 1.6b looks remarkably closer to theory.

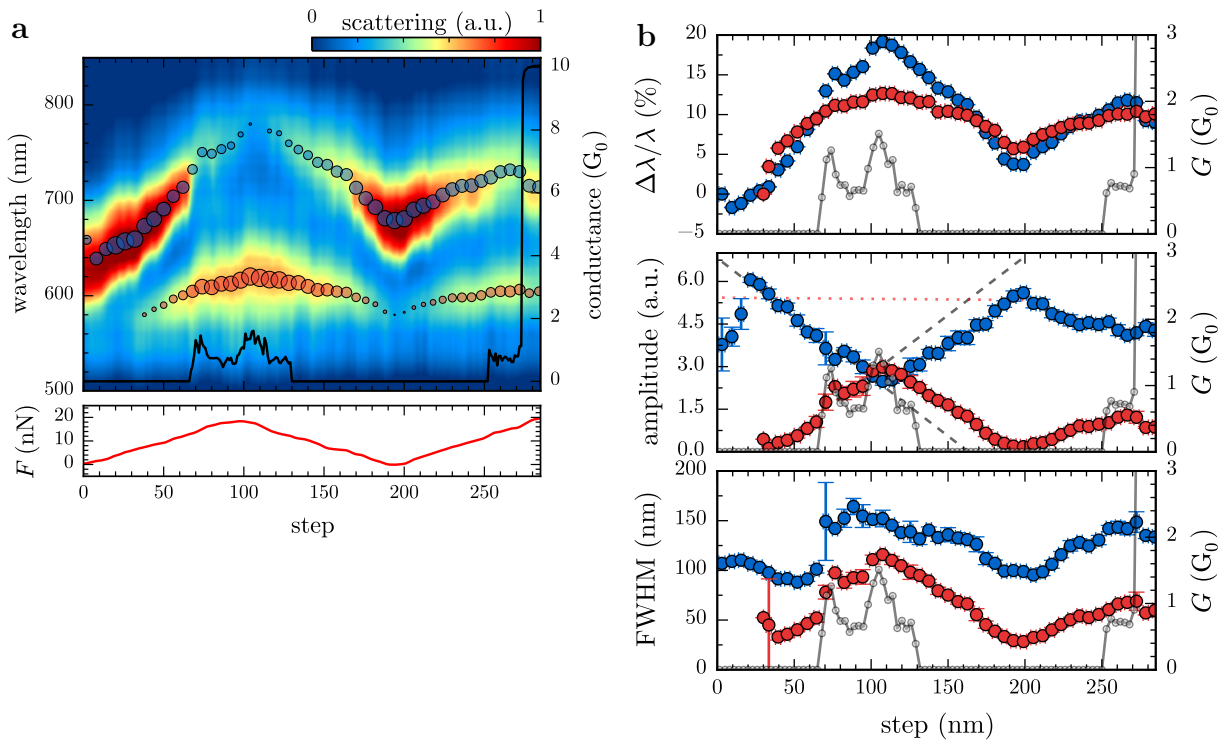


Figure 1.8: Detailed analysis of the extended electrochemically-fabricated spherical AuNP-on-Pt tip dimer scan. An extended plot of the scan shown in Figure 1.6c is plotted in (a), demonstrating reproducibility in approaches. The applied force trace represents separation changes between tips, with tips approached, retracted and then finally approached into geometrical contact. Peak positions in the fitted model are denoted by circles superimposed onto spectra with their size corresponding to the peak amplitude. The relative shift of each mode from fitted parameters, along with a normalised amplitude and FWHM, are plotted in (b). Reduced rates of redshift are found in the $G \sim 1G_0$ regions with a discontinuous blueshift seen after the $G > 2G_0$ transition. Linear rates of amplitude variation are revealed from peak fits after removing the width contribution from the peak intensity. A dotted red line shows the constant sum of the amplitudes. The FWHM of each mode increases with conductance.

Figure 1.6c shows a somewhat different phenomena to previous scans, though still in line with quantum transport expectations and bearing an interesting similarity with higher order plasmons in QCM spectra. Tips in Figure 1.6c are highly asymmetric AuNP-on-Pt tips, smoothed using piranha solution. Both cantilevers have 40 N m^{-1} spring constants, hence the force resolution during approach is limited. Prior to tunnelling a higher order mode begins to emerge. The transition into contact is quick, with few to zero points at any given conductance, ending initially with a stable $0.75\text{--}1.5G_0$ contact. The initial LSP resonance quickly diminishes with the rise of the conductance without blueshifting and the higher order resonance gains intensity. The screening here is another example of entering into a tunnelling regime but without sufficient current to enter into the conductive regime and form CTPs.

After the initial conductance increase, the tip is immediately retracted to test for reproducibility, as shown in the extended scan plot in Figure 1.8a. This is made possible by the

robustness of electrochemically fabricated tips, with their solid AuNP apices. Attempting this with commercial, spherical Au tips results in the spherical apex separating from the neck due to adhesion forces. A second approach of the tip immediately after retracting out of contact demonstrates the same phenomenon until the conductance rises above $2G_0$, at which point both modes blueshift. Changes in the redshift and amplitude gradient show the effects of surface morphology as retraction introduces a small degree of misalignment. This changes the conductance channels in the local electronic landscape and how they interact with the plasmon field.

A detailed mode analysis of plasmon resonances is shown in Figure 1.8b. Shifting of plasmon resonances behave as expected. Upon increasing the conductance up to the $1G_0$ level there is a visible reduction in the rate of redshift caused by screening. Once the conductance abruptly rises above $2G_0$ in the second approach there is a clear blueshift in the lowest order mode, alluding to a similar critical conductance. An interesting feature in this instance is that the extracted amplitude of the initial mode linearly decreases during approach at exactly the same rate as the new mode emerges. In a sense, charge is conserved and simply switches to a more favourable mode as the gap width decreases and tunnelling rate increases.

To summarise, each of the presented three scans shows agreement with recent theoretical concepts that predict the effects of quantum mechanical charge transfer on plasmon coupling. Four different plasmonic regimes related to charge transfer can be identified: classical coupling in the absence of charge transfer, a quantum tunnelling regime, a quantum (ballistic) conductive regime and, finally, a classical conductive regime. Tunnelling is responsible for screening whereas conductive contact leads to the progressive formation of CTPs. Critical conductances for entering the tunnelling regime and the quantum conductive regime are observed in each case in the vicinity of $2 \times 10^{-3}G_0$ and $2G_0$, respectively. This is the first time conductance values have been experimentally correlated with optical spectra using a dynamic approach to plasmon coupling.

Critical conductances are expected to hold outside of the quantum regime in the form of screening and CTP conductance thresholds. Comparison with previously explored systems shows excellent agreement, supporting the idea of a fixed set of critical conductances. Blueshifts of the BDP, forming the SBDP, begin to be seen in small $2G_0$ conductive contacts in both theoretical models [24, 26] and experimental NPoM systems when AuNPs are separated from a Au mirror by a blended SAM of variable conductance [25]. Observation of the same threshold conductance in two very different experimental systems provides strong evidence for the fundamental nature of critical conductances. Using this information, the plasmonics of a sub-nm plasmon system can begin to be better characterised and quantified with the aim to finally exploit plasmonics to measure optical conductivities.

1.4 Conclusions

Multiple different combinations of tips in a dimer configuration are used to probe plasmon coupling. Sharp Au tips exhibit no obvious plasmon resonances under far-field illumination and no gap mode coupling is observed with other sharp or spherical Au tips. This is caused by the lack of an antenna-like geometry in sharp tips. Plasmons excited at the apex of spherical Au tips, on the other hand, interact and hybridise. The behaviour of these modes is as expected, with similarity to plasmons in AuNP dimers. The inherent asymmetry between the large spherical tip structures leads to more complex scattering spectra wherein anti-bonding modes are no longer dark. Their spatial evolution into gap modes is something not previously seen before within a single plasmonic system.

To conclude experimental work, tip dimers are used to investigate the quantum regime of plasmonic coupling, specifically the effects of quantum charge transport. Using this approach, the development of the quantum regime is dynamically observed. Critical conductances are estimated for onset of each characteristic effect using direct correlations between optical spectra and current measurements. Measurements agree well with theoretical principles. Though no quantitative measurements, such as temperature, voltage or power dependences, are made to guarantee the exact mechanisms of charge transport, quantum tunnelling and ballistic conductance are the most likely mechanisms. Further investigation could quantify this, although charge transfer phenomena are not expected to depend on the specific conduction mechanism. Comparison with tip dimers coated in different molecular layers of varying conductivities would add further understanding into the effects of charge transfer and forms the basis of future experiments on this topic.

In summary, the existence of two distinct regimes of quantum charge transport have been detected in sub-nm plasmonic cavities. These are:

- The tunnelling regime (also known as the crossover regime), wherein electrons tunnelling through the barrier screen the capacitive interaction between opposite gap surfaces, reducing plasmon coupling strength and slowing the associated redshift to a halt.
- The conductive regime, where strong currents at G_0 -level conductances heavily attenuate gap plasmons and lead to the previously observed blueshift transition into charge transfer plasmons.

Though numerous theoretically predictions and experiments have been reported in recent years, this is the first time that correlated experimental measurements between plasmon resonances and conductance have been performed to understand quantum effects in plasmonic systems.

References

- [1] K. J. Savage et al., *Nature* **491**, 574–577 (2012).
- [2] Y. Gan, *Surface Science Reports* **64**, 99–121 (2009).
- [3] M. Holmberg et al., *Langmuir* **19**, 10510–10513 (2003).
- [4] Y. Song et al., *ChemPhysChem* **15**, 492–499 (2014).
- [5] Q Zhong et al., *Surface Science Letters* **290**, L688–L692 (1993).
- [6] P. Hansma et al., *Applied Physics Letters* **64**, 1738–1740 (1994).
- [7] C. A. Putman et al., *Applied physics letters* **64**, 2454–2456 (1994).
- [8] R. Esteban et al., *Faraday discussions* **178**, 151–183 (2015).
- [9] J. Lambe and S. McCarthy, *Physical Review Letters* **37**, 923 (1976).
- [10] R. Berndt, J. K. Gimzewski, and P. Johansson, *Physical review letters* **67**, 3796 (1991).
- [11] P. Bharadwaj, A. Bouhelier, and L. Novotny, *Physical review letters* **106**, 226802 (2011).
- [12] T Wang et al., *Nanotechnology* **22**, 175201 (2011).
- [13] S. Divitt, P. Bharadwaj, and L. Novotny, *Optics express* **21**, 27452–27459 (2013).
- [14] F. Ye et al., *Nanophotonics* **3**, 33–49 (2014).
- [15] P. Nordlander et al., *Nano Letters* **4**, 899–903 (2004).
- [16] A. Downes, D. Salter, and A. Elfick, *The Journal of Physical Chemistry B* **110**, 6692–6698 (2006).
- [17] J. T. Hugall, J. J. Baumberg, and S. Mahajan, *The Journal of Physical Chemistry C* **116**, 6184–6190 (2012).
- [18] J. Zuloaga, E. Prodan, and P. Nordlander, *Nano letters* **9**, 887–891 (2009).
- [19] R. Esteban et al., *Nature Communications* **3**, 825 (2012).
- [20] J. A. Scholl et al., *Nano letters* **13**, 564–569 (2013).
- [21] M. Barbry et al., *Nano letters* (2015).
- [22] S. F. Tan et al., *Science* **343**, 1496–1499 (2014).
- [23] G. Hajisalem, M. S. Nezami, and R. Gordon, *Nano letters* **14**, 6651–6654 (2014).
- [24] O Pérez-González, N Zabala, and J Aizpurua, *New Journal of Physics* **13**, 083013 (2011).
- [25] F. Benz et al., *Nano letters* **15**, 669–674 (2014).
- [26] O Pérez-González et al., *Nano letters* **10**, 3090–3095 (2010).